J|A|C|S ARTICLES

Published on Web 10/26/2010

Membrane Alignment of the Pore-Forming Component $TatA_d$ of the Twin-Arginine Translocase from *Bacillus subtilis* Resolved by Solid-State NMR Spectroscopy

Torsten H. Walther, Stephan L. Grage, Nadine Roth, and Anne S. Ulrich*

DFG-Center for Functional Nanostructures (CFN), Institute of Biological Interfaces (IBG-2), and Institute of Organic Chemistry, Karlsruhe Institute of Technology (KIT), Fritz-Haber-Weg 6, 76131 Karlsruhe, Germany

Received August 4, 2010; E-mail: anne.ulrich@kit.edu

Abstract: The twin-arginine translocase (Tat) provides protein export in bacteria and plant chloroplasts and is capable of transporting fully folded proteins across the membrane. We resolved the conformation and membrane alignment of the pore-forming subunit $TatA_d$ from *Bacillus subtilis* using solid-state NMR spectroscopy. The relevant structured part of the protein, $TatA_{2-45}$, contains a transmembrane segment (TMS) and an amphiphilic helix (APH). It was reconstituted in planar bicelles, which represent the lipid environment of a bacterial membrane. The SAMMY solid-state NMR experiment was used to correlate ^{15}N chemical shifts and $^{1}H-^{15}N$ dipolar couplings in the backbone and side chains of the ^{15}N-labeled protein. The observed wheel-like patterns ("PISA wheels") in the resulting 2-dimensional spectra confirm the α-helical character of the two segments and reveal their alignment in the lipid bilayer. Helix tilt angles ($\tau_{TMS} = 13°$, $\tau_{APH} = 64°$) were obtained from uniformly labeled protein, and azimuthal rotations ($\rho_{Val15} = 235°$, $\rho_{Ile29} = 25°$) were obtained from selective labels. These constraints define two distinct families of allowed structures for TatA in the membrane-bound state. The manifold of solutions could be narrowed down to a unique structure by using input from a liquid-state NMR study of TatA in detergent micelles, as recently described [Hu, Y.; Zhao, E.; Li, H.; Xia, B.; Jin, C. *J. Am. Chem. Soc.* **2010**, DOI: 10.1021/ja1053785]. Interestingly, the APH showed an unexpectedly slanted alignment in the protein, different from that of the isolated APH peptide. This finding implies that the amphiphilic region of TatA is not just a flexible attachment to the transmembrane anchor but might be able to form intra- or even intermolecular salt-bridges, which could play a key role in pore assembly.

Introduction

The export of proteins is an essential aspect of bacterial life and is often involved in the production of virulence factors. Besides the well-known Sec pathway, where unfolded proteins are threaded through a narrow translocation pore, there exists another pathway that is capable of transporting fully folded proteins.[1,2] Instead of being ATP-dependent, this twin-arginine translocation (Tat) pathway is driven by the proton electrochemical gradient across the membrane.[3−5] It is named after a characteristic twin-arginine consensus motif in the N-terminal signal peptide of the cargo proteins, by which they are targeted to the translocase.[6−9] This route was discovered in 1991 in plant thylakoids,[10] but little is known about the structure of the translocase subunits or the detailed mechanism of transport. The Tat system not only is present in plants but also plays a major role in bacteria and archea.[11−13] In bacteria, Tat-dependent transport was originally thought to be mainly responsible for the export of cofactor-containing proteins, but recently it has been shown that it is also associated with many other cellular processes,[13,14] like cell wall synthesis,[15−17] motility,[18,19] mem-

(1) Hynds, P. J.; Robinson, D.; Robinson, C. *J. Biol. Chem.* **1998**, *273*, 34868–34874.
(2) Robinson, C. *Biol. Chem.* **2000**, *381*, 89–93.
(3) Yahr, T. L.; Wickner, W. T. *EMBO J.* **2001**, *20*, 2472–2479.
(4) Braun, N. A.; Davis, A. W.; Theg, S. M. *Biophys. J.* **2007**, *93*, 1993–1998.
(5) Alami, M.; Trescher, D.; Wu, L. F.; Müller, M. *J. Biol. Chem.* **2002**, *277*, 20499–20503.
(6) Sargent, F.; Bogsch, E. G.; Stanley, N. R.; Wexler, M.; Robinson, C.; Berks, B. C.; Palmer, T. *EMBO J.* **1998**, *17*, 3640–3650.
(7) Chaddock, A. M.; Mant, A.; Karnauchov, I.; Brink, S.; Herrmann, R. G.; Klösgen, R. B.; Robinson, C. *EMBO J.* **1995**, *14*, 2715–2722.
(8) Berks, B. C. *Mol. Microbiol.* **1996**, *22*, 393–404.
(9) Wexler, M.; Bogsch, E. G.; Klösgen, R. B.; Palmer, T.; Robinson, C.; Berks, B. C. *FEBS Lett.* **1998**, *431*, 339–342.
(10) Mould, R. M.; Robinson, C. *J. Biol. Chem.* **1991**, *266*, 12189–12193.
(11) Yuan, J.; Zweers, J.; van Dijl, J.; Dalbey, R. *Cell. Mol. Life Sci.* **2009**, *67*, 179–199.
(12) Dilks, K.; Gimenez, M. I.; Pohlschröder, M. *J. Bacteriol.* **2005**, *187*, 8104–8113.
(13) Dilks, K.; Rose, R. W.; Hartmann, E.; Pohlschröder, M. *J. Bacteriol.* **2003**, *185*, 1478–1483.
(14) Berks, B. C.; Palmer, T.; Sargent, F. *Curr. Opin. Microbiol.* **2005**, *8*, 174–181.
(15) Ize, B.; Stanley, N. R.; Buchanan, G.; Palmer, T. *Mol. Microbiol.* **2003**, *48*, 1183–1193.
(16) Bernhardt, T. G.; Boer, P. A. J. d. *Mol. Microbiol.* **2003**, *48*, 1171–1182.
(17) Stanley, N. R.; Findlay, K.; Berks, B. C.; Palmer, T. *J. Bacteriol.* **2001**, *183*, 139–144.
(18) Ochsner, U. A.; Snyder, A.; Vasil, A. I.; Vasil, M. L. *Proc. Natl. Acad. Sci. U.S.A.* **2002**, *99*, 8312–8317.
(19) Ding, Z.; Christie, P. J. *J. Bacteriol.* **2003**, *185*, 760–771.

brane insertion of proteins,[20] and biofilm formation.[18,21] Its participation in the transport of virulence factors[21−26] and its absence in mammalian cells makes the Tat pathway a promising target for new antibiotics,[18,27,28] e.g. against *Salmonella enterica*, *Heliobacter pylorii*, *Mycobacterium tuberculosis*, and *Vibrio cholera*. In the context of drug design, it is important to obtain insight into the three-dimensional structure of the membrane-bound translocase machinery.

In *Escherichia coli* and most other Gram-negative bacteria, three types of integral membrane proteins, TatA, TatB, and TatC, are required for Tat-dependent transport.[6,13,29,30] *Bacillus subtilis*, however, possesses a simpler Tat system consisting of only TatA and TatC.[13,31] Several analogues of these proteins are present, which provide specific transport systems for the cargo proteins PhoD ($TatA_d$ and $TatC_d$) and YwbN ($TatA_y$ and $TatC_y$).[31−33] TatA is present in large excess[34] and thus is assumed to be the pore-forming component,[35] while TatC is probably responsible for the initial recognition of the signal peptide.[36−39] It has been shown by electron microscopy that TatA can self-assemble into ring-like structures[35,40,41] and that the TatBC complexes bind the signal peptide.[42] Detailed molecular structures, however, are still missing. For TatC, a topology with four to six transmembrane α-helices has been proposed,[43,44] with a high α-helical content and a predominantly transmembrane orientation according to circular dichroism (CD) spectroscopy and oriented CD (OCD).[45]

Sequence analysis predicts that the pore-forming subunit TatA consists of an N-terminal transmembrane segment (TMS), an amphiphilic helix (APH), and an unstructured C-terminus.[46,47] In a previous study, we used a reductionist approach to examine various fragments of the 70 amino acid protein $TatA_d$ from *B. subtilis* in liposomes and in macroscopically oriented lipid bilayers. CD confirmed the presence of the two α-helical segments and an unstructured C-terminus, and OCD supported the transmembrane orientation of the TMS and the surface alignment of the APH.[48] The orientation of the TMS was characterized using solid-state NMR in planar bicelles as a membrane-mimicking environment.[49] In the accompanying paper,[50] Hu et al. have now determined the structure of $TatA_d$ in detergent micelles by liquid-state NMR. The nuclear Overhauser effect signals (NOEs) provided detailed short-range constraints on the protein conformation, and residual dipolar couplings (RDCs) were used to reveal its global geometry. However, the alignment of the protein in the membrane can only be determined by solid-state NMR.

Bicelles represent a suitable membrane environment for solid-state NMR structure analysis. Consisting of mixtures of long- and short-chain lipids,[51] they are used to provide a flat bilayer for the reconstitution of transmembrane proteins,[52,53] in contrast to highly curved detergent micelles. The membrane normal of the usual "unflipped" bicelles is oriented perpendicular to the magnetic field. Doping with lanthanide ions results in "flipped" bicelles, whose membrane normal is parallel to the magnetic field.[54−56] High-resolution two-dimensional separated local field methods like polarization inversion spin exchange at the magic angle (PISEMA)[57] or SAMMY[58,59] on a uniformly ^{15}N-labeled protein can then reveal the orientation of a helical segment with respect to the bilayer plane, simply by inspection of the resonance patterns, the so-called "PISA wheels" (where PISA means *p*olarity *i*ndex *s*lant *a*ngle).[60] The angle τ describes the

(20) De Buck, E.; Vranckx, L.; Meyen, E.; Maes, L.; Vandersmissen, L.; Anne, J.; Lammertyn, E. *FEBS Lett.* **2007**, *581*, 259–264.
(21) Zhang, L.; Zhu, Z.; Jing, H.; Zhang, J.; Xiong, Y.; Yan, M.; Gao, S.; Wu, L. F.; Xu, J.; Kan, B. *BMC Microbiol.* **2009**, *9*, 114.
(22) McDonough, J. A.; McCann, J. R.; Tekippe, E. M.; Silverman, J. S.; Rigel, N. W.; Braunstein, M. *J. Bacteriol.* **2008**, *190*, 6428–6438.
(23) De Buck, E.; Hoper, D.; Lammertyn, E.; Hecker, M.; Anne, J. *Int. J. Med. Microbiol.* **2008**, *298*, 449–461.
(24) De Buck, E.; Maes, L.; Meyen, E.; Van Mellaert, L.; Geukens, N.; Anne, J.; Lammertyn, E. *Biochem. Biophys. Res. Commun.* **2005**, *331*, 1413–1420.
(25) De Buck, E.; Lebeau, I.; Maes, L.; Geukens, N.; Meyen, E.; Van Mellaert, L.; Anne, J.; Lammertyn, E. *Biochem. Biophys. Res. Commun.* **2004**, *317*, 654–661.
(26) McDonough, J. A.; Hacker, K. E.; Flores, A. R.; Pavelka, M. S., Jr.; Braunstein, M. *J. Bacteriol.* **2005**, *187*, 7667–7679.
(27) De Buck, E.; Lammertyn, E.; Anne, J. *Trends Microbiol.* **2008**, *16*, 442–453.
(28) Lavander, M.; Ericsson, S. K.; Broms, J. E.; Forsberg, A. *Adv. Exp. Med. Biol.* **2007**, *603*, 258–267.
(29) Sargent, F.; Stanley, N. R.; Berks, B. C.; Palmer, T. *J. Biol. Chem.* **1999**, *274*, 36073–36082.
(30) Bogsch, E. G.; Sargent, F.; Stanley, N. R.; Berks, B. C.; Robinson, C.; Palmer, T. *J. Biol. Chem.* **1998**, *273*, 18003–18006.
(31) Jongbloed, J. D. H.; Grieger, U.; Antelmann, H.; Hecker, M.; Nijland, R.; Bron, S.; Dijl, J. M. v. *Mol. Microbiol.* **2004**, *54*, 1319–1325.
(32) Jongbloed, J. D.; Antelmann, H.; Hecker, M.; Nijland, R.; Bron, S.; Airaksinen, U.; Pries, F.; Quax, W. J.; van Dijl, J. M.; Braun, P. G. *J. Biol. Chem.* **2002**, *277*, 44068–44078.
(33) Pop, O.; Martin, U.; Abel, C.; Müller, J. P. *J. Biol. Chem.* **2002**, *277*, 3268–3273.
(34) Jack, R. L.; Sargent, F.; Berks, B. C.; Sawers, G.; Palmer, T. *J. Bacteriol.* **2001**, *183*, 1801–1804.
(35) Sargent, F.; Gohlke, U.; De Leeuw, E.; Stanley, N. R.; Palmer, T.; Saibil, H. R.; Berks, B. C. *Eur. J. Biochem.* **2001**, *268*, 3361–3367.
(36) Cline, K.; Mori, H. *J. Cell Biol.* **2001**, *154*, 719–729.
(37) Allen, S. C.; Barrett, C. M.; Ray, N.; Robinson, C. *J. Biol. Chem.* **2002**, *277*, 10362–10366.
(38) de Leeuw, E.; Granjon, T.; Porcelli, I.; Alami, M.; Carr, S. B.; Müller, M.; Sargent, F.; Palmer, T.; Berks, B. C. *J. Mol. Biol.* **2002**, *322*, 1135–1146.
(39) Alami, M.; Luke, I.; Deitermann, S.; Eisner, G.; Koch, H. G.; Brunner, J.; Müller, M. *Mol. Cell* **2003**, *12*, 937–946.
(40) Gohlke, U.; Pullan, L.; McDevitt, C. A.; Porcelli, I.; de Leeuw, E.; Palmer, T.; Saibil, H. R.; Berks, B. C. *Proc. Natl. Acad. Sci. U.S.A.* **2005**, *102*, 10482–10486.
(41) Westermann, M.; Pop, O. I.; Gerlach, R.; Appel, T. R.; Schlormann, W.; Schreiber, S.; Müller, J. P. *Biochim. Biophys. Acta* **2006**, *1758*, 443–451.
(42) Tarry, M. J.; Schafer, E.; Chen, S.; Buchanan, G.; Greene, N. P.; Lea, S. M.; Palmer, T.; Saibil, H. R.; Berks, B. C. *Proc. Natl. Acad. Sci. U.S.A.* **2009**, *106*, 13284–13289.
(43) Punginelli, C.; Maldonado, B.; Grahl, S.; Jack, R.; Alami, M.; Schröder, J.; Berks, B. C.; Palmer, T. *J. Bacteriol.* **2007**, *189*, 5482–5494.
(44) Gouffi, K.; Santini, C.-L.; Wu, L.-F. *FEBS Lett.* **2002**, *525*, 65–70.
(45) Nolandt, O. V.; Walther, T. H.; Roth, S.; Bürck, J.; Ulrich, A. S. *Biochim. Biophys. Acta* **2009**, *1788*, 2238–2244.
(46) Palmer, T.; Berks, B. C. *Microbiology* **2003**, *149*, 547–556.
(47) Porcelli, I.; de Leeuw, E.; Wallis, R.; van den Brink-van der Laan, E.; de Kruijff, B.; Wallace, B. A.; Palmer, T.; Berks, B. C. *Biochemistry* **2002**, *41*, 13690–13697.
(48) Lange, C.; Müller, S. D.; Walther, T. H.; Bürck, J.; Ulrich, A. S. *Biochim. Biophys. Acta* **2007**, *1768*, 2627–2634.
(49) Müller, S. D.; De Angelis, A. A.; Walther, T. H.; Grage, S. L.; Lange, C.; Opella, S. J.; Ulrich, A. S. *Biochim. Biophys. Acta* **2007**, *1768*, 3071–3079.
(50) Hu, Y.; Zhao, E.; Li, H.; Xia, B.; Jin, C. *J. Am. Chem. Soc.* **2010**, ASAP (DOI: 10.1021/ja1053785).
(51) Sanders, C. R.; Schwonek, J. P. *Biochemistry* **1992**, *31*, 8898–8905.
(52) De Angelis, A. A.; Opella, S. J. *Nat Protoc* **2007**, *2*, 2332–2338.
(53) Sanders, C. R., II.; Landis, G. C. *Biochemistry* **1995**, *34*, 4030–4040.
(54) Prosser, R. S.; Hunt, S. A.; DiNatale, J. A.; Vold, R. R. *J. Am. Chem. Soc.* **1996**, *118*, 269–270.
(55) Howard, K. P.; Opella, S. J. *J. Magn. Reson. B* **1996**, *112*, 91–94.
(56) Prosser, R. S.; Hwang, J. S.; Vold, R. R. *Biophys. J.* **1998**, *74*, 2405–2418.
(57) Wu, C. H.; Ramamoorthy, A.; Opella, S. J. *J. Magn. Reson. Ser. A* **1994**, *109*, 270–272.
(58) Nevzorov, A. A.; Opella, S. J. *J. Magn. Reson.* **2003**, *164*, 182–186.
(59) Nevzorov, A. A.; Opella, S. J. *J. Magn. Reson.* **2007**, *185*, 59–70.
(60) Wang, J.; Denny, J.; Tian, C.; Kim, S.; Mo, Y.; Kovacs, F.; Song, Z.; Nishimura, K.; Gan, Z.; Fu, R.; Quine, J. R.; Cross, T. A. *J. Magn. Reson.* **2000**, *144*, 162–167.

tilt of the helix axis away from the membrane normal, and the azimuthal angle ρ defines the rotation around the helix (at the Cα atom of a specified residue). Additionally, a so-called molecular order parameter, $0 \leq S_{mol} \leq 1$, can be included to describe the extent of motional averaging, ranging from complete isotropic tumbling ($S_{mol} = 0$) to the absence of any wobbling ($S_{mol} = 1.0$). We have previously determined the tilt angle of the TatA$_d$ TMS as $\tau = 17° \pm 3°$, and from a selectively ^{15}N-valine-labeled protein we found the rotation angle ρ_{Val15} to be approximately 215°, with $S_{mol} = 0.8$ being typical of a monomeric transmembrane helix.[49] The limited resolution of the solid-state NMR signals from the APH, however, precluded obtaining any further structural information about this region. Using several different amino acid type-selective labeled samples together with flipped bicelles, we are now able to present the membrane alignment of the amphiphilic part of the protein when connected to the TMS. With the assignment of all TMS signals, the necessary constraints are now available to align the two constituent helical segments of TatA$_d$ in the membrane, which is an important step toward obtaining a comprehensive picture with atomic resolution. On the basis of solid-state NMR data alone, the relative alignment of the two helices with respect to one another cannot be unambiguously determined, and a family of possible structures emerges. However, according to the liquid-state NMR data in the accompanying paper by Hu et al.,[50] the angle between the two helices is known and can be used to derive a unique solution from the solid-state NMR constraints. We are thus able to present a complete three-dimensional picture of the folding and alignment of the TatA protein in its monomeric membrane-bound state.

A remarkable feature of these results is the observation that the APH assumes a comparatively steep tilt angle in the membrane (rather than lying flat on the surface), and its azimuthal rotation places some polar residues sideways. To address its functional role in the protein, we have therefore also analyzed the APH as an isolated peptide fragment, whereupon it reverted to the typical behavior of a passively surface-bound amphiphilic helix. These findings suggest that the presence of the TMS has a pronounced influence on the orientation of the polar part of the protein and that the amphiphilic region may play a role in the self-assembly of the TatA pore, possibly by the formation of salt-bridges.

Results

To characterize the orientation of the APH by solid-state NMR, we used the construct TatA$_{2-45}$, which contains only the TMS and APH of the protein TatA$_d$ from *B. subtilis*. It has been shown that some C-terminally truncated mutants are still transport competent,[61,62] and we have previously demonstrated by CD spectroscopy that the C-terminus of the membrane-bound protein is unstructured from about Ser$_{46}$ onward.[48] Likewise, it was confirmed by liquid-state NMR methods that the full-length protein in detergent micelles has an increasingly dynamic APH from Lys$_{41}$ to Val$_{48}$, which becomes completely unstructured in the rest of the C-terminus.[50] As illustrated in our previous solid-state NMR study on the orientation of the TMS,[49] the truncated TatA$_{2-45}$ showed much better orientation in bicelles and less aggregation than the full 70 amino acid protein. Furthermore, it is known that C-terminal backbone sites that are highly mobile on the time scale of the ^{1}H$-^{15}$N dipolar coupling and the ^{15}N chemical shift would give rise to signals with 0 kHz dipolar coupling and an isotropic chemical shift.[63] Since we may also expect to find the signals of a slightly tilted APH in this spectral region, the strong signals of the unstructured C-terminus would interfere and make an assignment much more complicated.

^{31}P NMR of the Bicelles and ^{15}N NMR of TatA$_{2-45}$. For a membrane-mimicking environment we used bicelles ($q = 3.2$, 22% total lipids) composed of charged and uncharged long-chain phospholipids [80 mol % 1,2-dimyristoyl-*sn*-glycero-3-phosphocholine (DMPC) and 20 mol % 1,2-dimyristoyl-*sn*-glycero-3-[phospho-*rac*-(1-glycerol)], sodium salt (DMPG)], plus the ether-linked 1,2-di-*O*-hexyl-*sn*-glycero-3-phosphocholine (6-O-PC) as short-chain lipid in order to increase stability.[64,65] The ^{31}P NMR spectra show that the reconstituted protein does not disturb the orientation of the bicelles (Figure 1A,C). In the case of the unflipped bicelles (Figure 1A), the two most upfield-shifted signals are assigned to the long-chain lipids DMPC and DMPG,[51] whose molecular axes are oriented perpendicular to the magnetic field $\mathbf{B}_0$. The signal from 6-O-PC occurs close to the isotropic position due to the fast diffusion of this short-chain lipid around the rim of the bicelles.[66,67] Adding $YbCl_3$ to a final concentration of 3 mM resulted in flipped bicelles (Figure 1C). The lanthanide ions with their high positive magnetic susceptibility bind to lipid headgroups and turn the orientation of the bicelles perpendicular to the magnetic field.[54−56] This leads to a doubling of the spectral width, which can lead to an increase spectral resolution, provided that the line width does not increase proportionally.[68] In the present case of the ^{31}P NMR spectrum, the resolution is not improved, yet these spectra show that the flipped bicelles are well oriented: the signals are shifted downfield, indicating that the bilayer normal is now oriented parallel to the magnetic field.

The TatA$_{2-45}$ protein is very well aligned in the bicelles, as seen from the high resolution of the ^{15}N NMR spectra (Figure 1B,D]. In unflipped bicelles, narrow NMR signals are obtained only when the reconstituted protein performs fast rotational diffusion around the bilayer normal. In the absence of this diffusive motion, the spectra would contain a partial powder pattern incompatible with obtaining high-resolution spectra.[69,70] The sharp lines in Figure 1D thus indicate that we are dealing with TatA monomers here, rather than a TatA complex or an oligomeric pore, as supported by analogous experiments with oriented samples on glass plates (data not shown). The ^{15}N NMR signals are grouped into two distinct spectral regions. In the unflipped bicelles (Figure 1B), the upfield signals with 80−95 ppm chemical shift originate from amide ^{15}N-CSA tensors lying with their long axis approximately parallel to the bilayer normal,

(61) Lee, P. A.; Buchanan, G.; Stanley, N. R.; Berks, B. C.; Palmer, T. *J. Bacteriol.* **2002**, *184*, 5871–5879.
(62) Dabney-Smith, C.; Mori, H.; Cline, K. *J. Biol. Chem.* **2003**, *278*, 43027–43033.
(63) Marassi, F. M.; Ramamoorthy, A.; Opella, S. J. *Proc. Natl. Acad. Sci. U.S.A.* **1997**, *94*, 8551–8556.
(64) Aussenac, F.; Lavigne, B.; Dufourc, E. J. *Langmuir* **2005**, *21*, 7129–7135.
(65) Ottiger, M.; Bax, A. *J. Biomol. NMR* **1999**, *13*, 187–191.
(66) Picard, F.; Paquet, M. J.; Levesque, J.; Belanger, A.; Auger, M. *Biophys. J.* **1999**, *77*, 888–902.
(67) Marcotte, I.; Auger, M. *Concept. Magn. Reson. Part A* **2005**, *24A*, 17–37.
(68) Park, S. H.; Loudet, C.; Marassi, F. M.; Dufourc, E. J.; Opella, S. J. *J. Magn. Reson.* **2008**, *193*, 133–138.
(69) Park, S. H.; Mrse, A. A.; Nevzorov, A. A.; De Angelis, A. A.; Opella, S. J. *J. Magn. Reson.* **2006**, *178*, 162–165.
(70) De Angelis, A. A.; Nevzorov, A. A.; Park, S. H.; Howell, S. C.; Mrse, A. A.; Opella, S. J. *J. Am. Chem. Soc.* **2004**, *126*, 15340–15341.

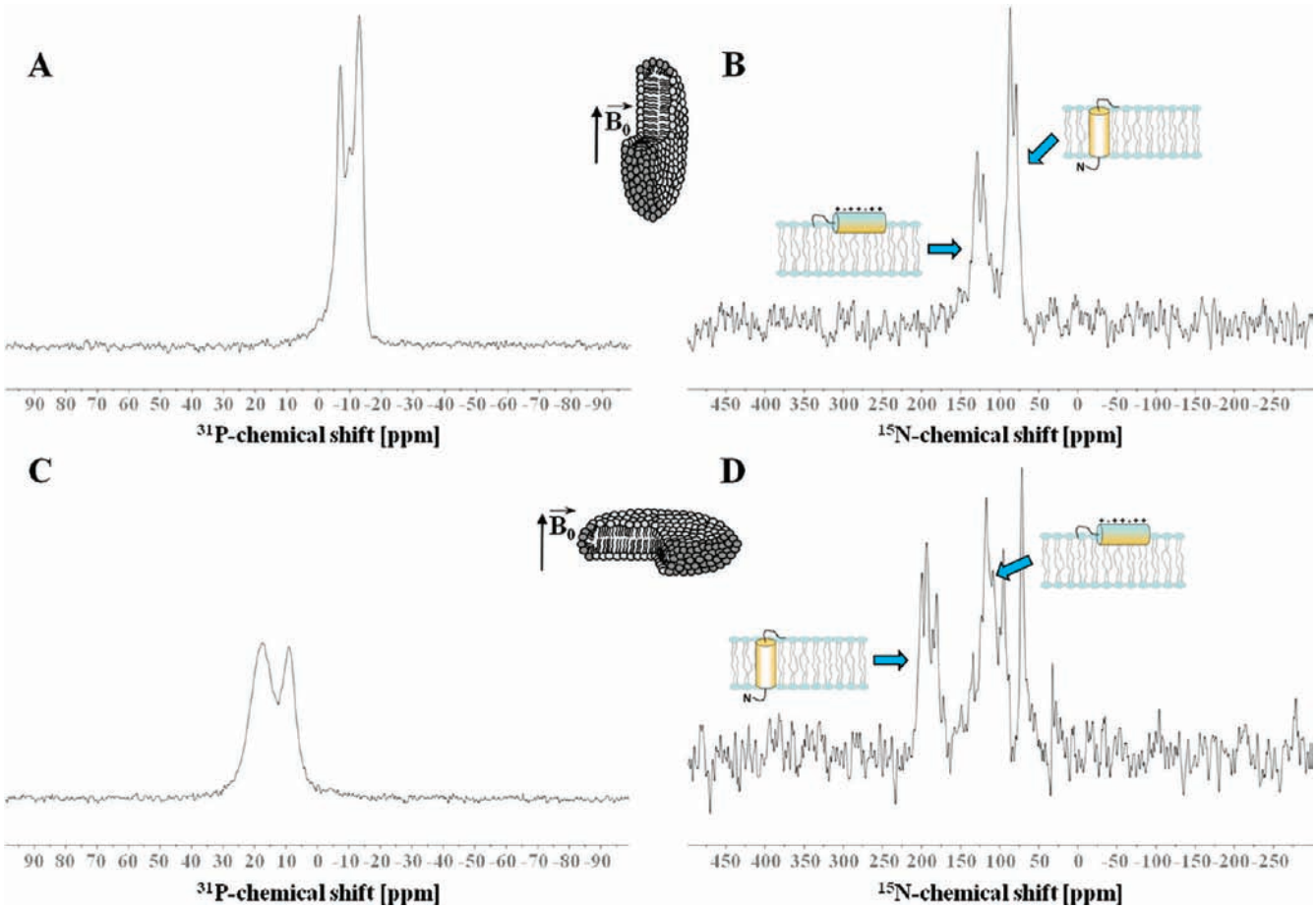

Figure 1. ^{31}P NMR (A,C) and ^{15}N NMR (B,D) of unflipped (A,B) and flipped (C,D) DMPC/DMPG/6-O-PC-bicelles containing uniformly ^{15}N-labeled $TatA_{2-45}$ (q = 3.2, 22% total lipid, peptide-to-lipid ratio P:L = 1:100, pH = 6.8, T = 315 K).

and hence they can be assigned to the TMS. The downfield signals in the region of 110−135 ppm are assigned to the APH, which is significantly tilted. Upon flipping the bicelles (Figure 1D), the spectral width is doubled and resolution is improved, as the ^{15}N NMR line widths did not increase proportionally (unlike the ^{31}P NMR data). The signals of the TMS shifted downfield to 175−205 ppm, and the signals of the APH moved to 100−140 ppm and show increased intensity. Furthermore, three sharp and strong signals at about 30, 75, and 90 ppm can be identified, which must arise from mobile parts of the protein, probably from the nitrogen-containing side chains. These signals stay nearly at the same position upon flipping and can thus be assigned by comparison with the known isotropic chemical shifts of the respective residues. The signal at 30 ppm (which is barely observable in the unflipped sample) is characteristic of the N-terminus or the lysine side chains.[63,71,72] The signals at 75 and 90 ppm, which overlap with the signals of the TMS in the case of the unflipped sample, most likely belong to the two primary and the secondary amine moieties of the arginine side chains.[71,72] The protein $TatA_{2-45}$ contains also an asparagine, whose side-chain signal probably overlaps with the signals of the APH in both unflipped and flipped bicelles.

2D NMR of Uniformly ^{15}N-Labeled $TatA_{2-45}$ in Bicelles To Obtain the Helix Tilt Angles. To resolve the NMR signals in a second spectral dimension, we used the two-dimensional separated local field experiment SAMMY, which has a reduced frequency offset dependence and is easier to set up compared to PISEMA.[58,59] It correlates the amide ^{15}N chemical shift with the ^{1}H−^{15}N dipolar coupling, and α-helices yield spectra with characteristic wheel-like patterns due to their periodicity. Such PISA wheels directly map the helical wheel projection, as each amide group in the peptide backbone generates a discrete signal. The position and size of the PISA wheel in the spectrum provide quantitative information about the orientation and wobbling of the helical segment in the magnetic field. The tilt angle τ of the helix and its order parameter S_{mol} in the membrane can be determined simply by comparison with simulated spectra based on an ideal α-helix.[60] As our construct $TatA_{2-45}$ contains a transmembrane and an amphiphilic helix, two PISA wheels are expected. In Figure 2, the SAMMY spectra of $TatA_{2-45}$ in unflipped and flipped bicelles are presented. One well-resolved PISA wheel is observed around 80−95 ppm ^{15}N chemical shift and 2.5−3.9 kHz ^{1}H−^{15}N dipolar coupling in unflipped bicelles. In flipped bicelles these signals have moved to 175−205 ppm and to 5−7.8 kHz, respectively. This PISA wheel can be clearly assigned to the transmembrane helix,[49] as the signals arise from amide tensors lying parallel to the bicelle normal.

Representing the APH, a second group of signals is seen around 110−135 ppm and 0−1 kHz in the unflipped bicelles, which upon flipping move to 100−140 ppm and 0−2 kHz, respectively. However, the couplings are intrinsically smaller in this region of the spectrum, and the ^{1}H−^{15}N dipolar coupling changes its sign (as colored in red and green in Figure 2A,B).

(71) Biological Magnetic Resonance Data Bank, http://www.bmrb.wisc.edu/ref_info/statsel.htm#2; 01.02.2010.
(72) Ulrich, E. L.; et al. *Nucleic Acids Res.* **2008**, *36*, D402–408.

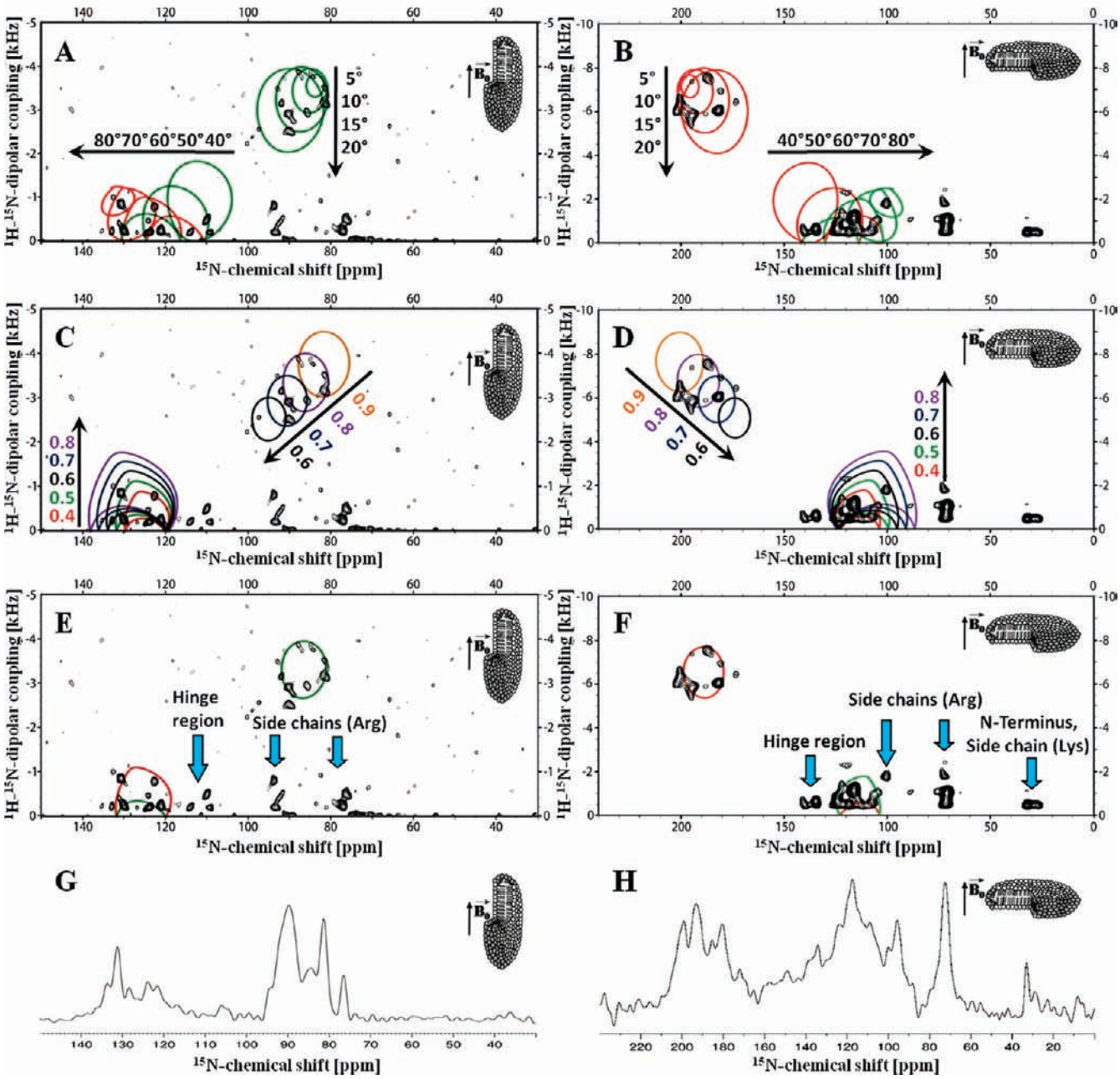

Figure 2. SAMMY spectra of uniformly ^{15}N-labeled TatA$_{2-45}$ in unflipped (A,C,E,G) and flipped (B,D,F,H) bicelles acquired under the same conditions as in Figure 1. (A,B) Overlay of simulated PISA wheels with varying tilt angle τ (TMS, $\tau = 5° \rightarrow 20°$, $S_{mol} = 0.8$; APH, $\tau = 40° \rightarrow 80°$, $S_{mol} = 0.5$). (C,D) Overlay of simulated PISA wheels with varying order parameter S_{mol} (TMS, $\tau = 13°$, $S_{mol} = 0.6 \rightarrow 0.9$; APH, $\tau = 64°$, $S_{mol} = 0.4 \rightarrow 0.8$). (E,F) Overlay of the best-fit simulated PISA wheel (TMS, $\tau = 13°$, $S_{mol} = 0.8$; APH, $\tau = 64°$, $S_{mol} = 0.5$ for unflipped and 0.4 for flipped bicelles). (G,H) One-dimensional ^{15}N NMR spectra of ^{15}N-labeled TatA$_{2-45}$.

Therefore, the PISA wheel is less readily discernible, especially as it looks like a double-winged pattern (as in Figure 2E,F). Computation shows that a helix with a tilt angle of about 50−70° produces signals in this region of the spectrum, which is indicative of a tilted APH segment of TatA. A close look at the simulated PISA wheels for different values of τ and S_{mol} (Figure 2A−D) nevertheless shows that there does not exist a perfect fit that can account for all of the signals in this region. It is thus likely that these signals arise not only from the APH but also from the hinge region between the APH and TMS. The remaining signals in Figure 2E,F, around 30 ppm (visible only in the flipped bicelles) and at 75 and 95 ppm, can be assigned to the N-terminus/lysine side chain and to the arginine side chains, as noted above. The fact that these signals show a slight shift upon flipping suggests that the side chains are not completely isotropic but retain a residual orientation in the membrane. The simulations with the best fit (Figure 2E,F) show that the TMS is tilted by 13° ± 4° with an order parameter of $S_{mol} = 0.8$, and the APH has a tilt of $\tau = 64° \pm 10°$ and a smaller S_{mol} around 0.5.

2D NMR of Selectively Labeled TatA$_{2-45}$ To Obtain the Helix Rotation Angles. To determine the azimuthal rotation angle ρ of a helix, the SAMMY spectra need to be assigned. Due to the periodicity of α-helices, it is in principle possible to assign a complete PISA wheel from a single selectively ^{15}N-labeled sample. To confirm the above spectral interpretations, especially regarding the APH, we prepared several TatA$_{2-45}$ samples with different amino acid type-selective labels. For example, there

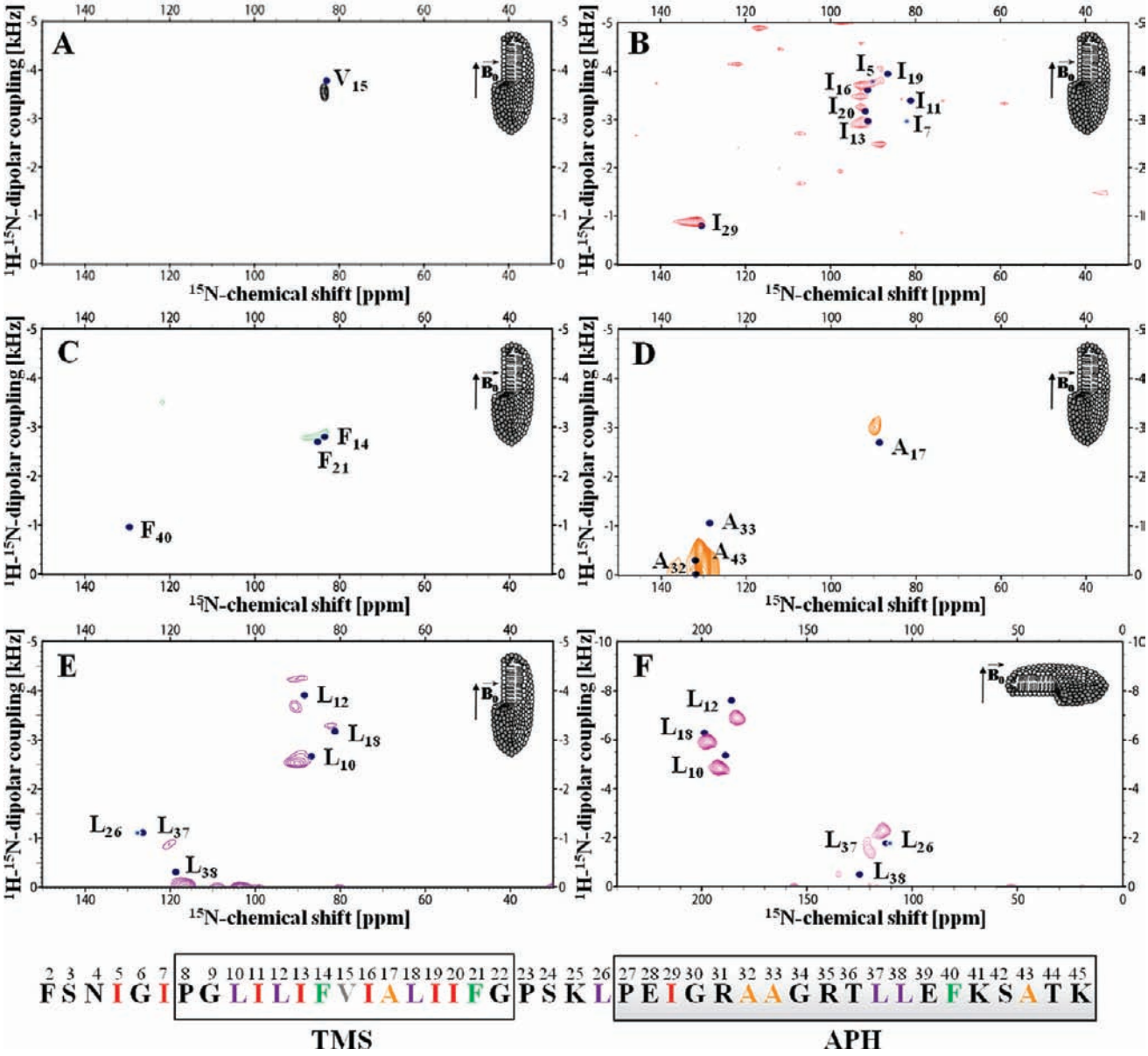

Figure 3. SAMMY spectra of selectively ^{15}N-labeled $TatA_{2-45}$ in unflipped (A−E) and flipped (F) bicelles. (A) ^{15}N-Val labeling and overlay of simulation (TMS, $\tau = 13°$, $S_{mol} = 0.8$, $\rho_{Val15} = 235°$). (B) ^{15}N-Ile labeling and overlay with simulation (TMS, $\tau = 13°$, $S_{mol} = 0.8$, $\rho_{Ile5} = 315°$, $\rho_{Ile7} = 155°$, $\rho_{Ile11} = 195°$, $\rho_{Ile13} = 35°$, $\rho_{Ile16} = 335°$, $\rho_{Ile19} = 275°$, $\rho_{Ile20} = 15°$; APH, $\tau = 64°$, $S_{mol} = 0.5$, $\rho_{Ile29} = 25°$). (C) ^{15}N-Phe labeling and overlay with simulation (TMS, $\tau = 13°$, $S_{mol} = 0.8$, $\rho_{Phe14} = 135°$, $\rho_{Phe21} = 115°$; APH, $\tau = 64°$, $S_{mol} = 0.5$, $\rho_{Phe40} = 45°$). (D) ^{15}N-Ala labeling and overlay with simulation (TMS, $\tau = 13°$, $S_{mol} = 0.8$, $\rho_{Ala17} = 75°$; APH, $\tau = 64°$, $S_{mol} = 0.5$, $\rho_{Ala32} = 325°$, $\rho_{Ala33} = 65°$, $\rho_{Ala43} = 345°$). (E,F) ^{15}N-Leu labeling in unflipped and flipped bicelles, and overlay with simulation (TMS, $\tau = 13°$, $S_{mol} = 0.8$, $\rho_{Leu10} = 95°$, $\rho_{Leu12} = 295°$, $\rho_{Leu18} = 175°$; APH, $\tau = 64°$, $S_{mol} = 0.5$ for unflipped and 0.4 for flipped bicelles, $\rho_{Leu26} = 85°$, $\rho_{Leu37} = 105°$, $\rho_{Leu38} = 205°$).

is a single valine in the protein, and the corresponding SAMMY spectrum contains only one signal in the region of the TMS PISA wheel. This assignment yields a rotation angle of $\rho_{Val15} = 235°$ for the transmembrane helix (Figure 3A). Due to the periodicity of an ideal α-helix, the azimuthal angles of all other amino acids in the TMS are fixed. Their expected position in the spectrum can thus be calculated and verified experimentally to detect any deviations, e.g. due to local distortions of the helical structure. For these simulations (based on $\tau = 13°$ and $S_{mol} = 0.8$ for the TMS, and see below for the APH), a home-written program was used.

To aid further assignment, we estimated the length of the hydrophobic TMS using a D_2O exchange experiment on uniformly ^{15}N-labeled $TatA_{2-45}$ in SDS micelles by liquid-state NMR (see Supporting Information, Figure S1). The TMS is found to be flanked by Gly_9 and Gly_{22}, whose signals are still visible after D_2O addition but disappear within hours. The stretch from Leu_{10} to Phe_{21}, on the other hand, remains inaccessible in the hydrophobic micelle core for several weeks. According to this definition of the TMS, the selectively ^{15}N-isoleucine-labeled protein should give rise to five signals in the TMS region of the SAMMY spectrum, as is seen in Figure 3B. The predicted signals of Ile_{13}, Ile_{16}, Ile_{19}, and Ile_{20} fit the experimental data well, and only the signal of Ile_{11} is so weak that it may nearly not be discriminated over the noise. However, there are still two signals left in this region of the spectrum, so we also included Ile_5 and Ile_7 in our calculation of the PISA positions to allow for the possibility that the TMS helix might be longer in the bicelles than in the highly curved and dynamic micelles. Indeed, one of these signals (light blue in Figure 3B) fits well

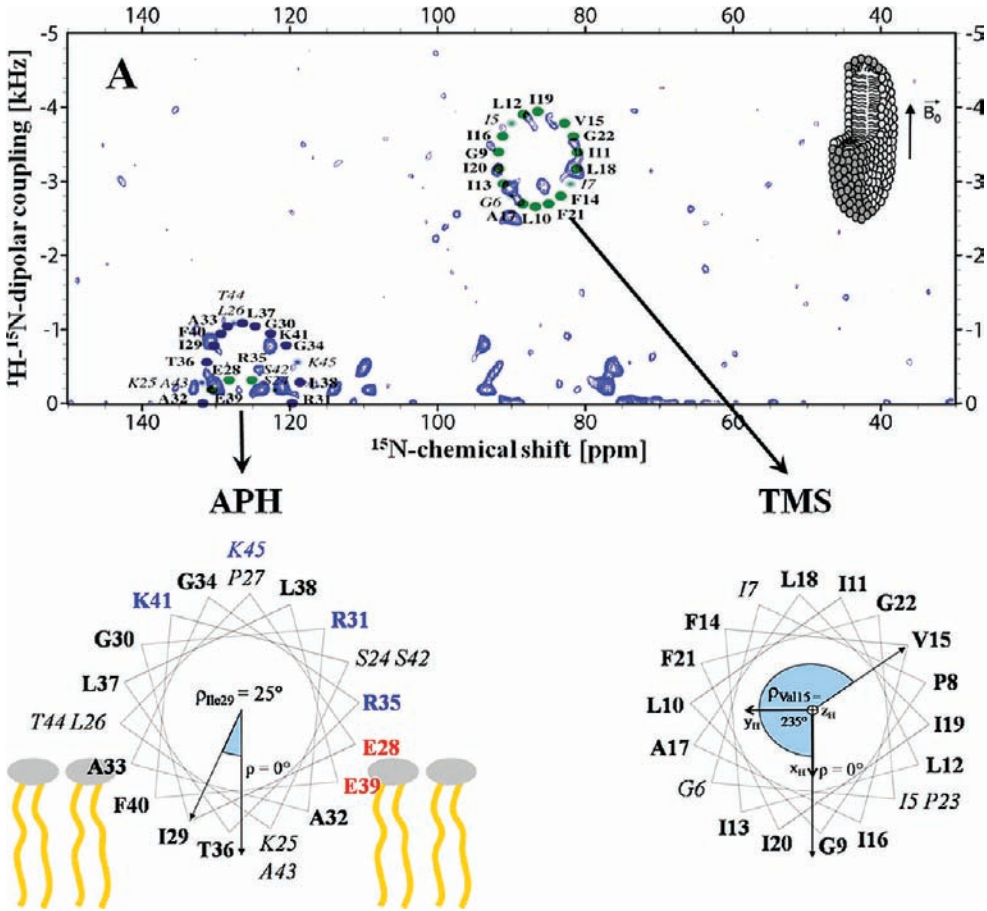

Figure 4. SAMMY spectrum of uniformly ^{15}N-labeled $TatA_{2-45}$ in unflipped bicelles, overlaid with PISA wheels that have been computed according to the assignment by amino acid type-selective labeling (TMS, $\tau = 13°$, $S_{mol} = 0.8$, $\rho_{Val15} = 235°$; APH, $\tau = 64°$, $S_{mol} = 0.5$, $\rho_{Ile29} = 25°$). The resulting alignment of the two helical segments in the lipid bilayer is illustrated.

the calculated signal of Ile_5. The remaining signal at 90 ppm is then assigned to Ile_7. The fact that it does not fit so well to the calculated signal might be explained by a slight local distortion of the helical structure at this position, as Ile_7 precedes the helix-breaking residue Pro_8. In the APH, $TatA_{2-45}$ possesses only a single isoleucine residue, which is an essential clue for determining the azimuthal rotation angle unambiguously for the APH. The SAMMY spectrum for ^{15}N-Ile shows a single well-resolved signal in the APH region as expected, and the simulated PISA wheel with $\tau = 64°$, $S_{mol} = 0.5$ yields a rotation angle of $\rho_{Ile29} = 25°$. Allowing for some larger deviations from the τ and S_{mol} values that had been deduced from the uniformly labeled sample, the second-best possibility to fit the single signal in spectrum B in Figure 3would correspond to a somewhat different set of parameters with $\tau = 55°$, $S_{mol} = 0.7$, $\rho_{Ile29} = 325°$ (Supporting Information, Figures S2 and S3, but see discussion below).

Assignment continues with the SAMMY spectrum of ^{15}N-Phe-labeled $TatA_{2-45}$, which shows a broad peak in the region of the TMS (Figure 3C) that fits well to the calculated signals for the two transmembrane phenylalanine residues. In the APH region, we would expect one signal for Phe_{40}, but none is visible here. Likewise, the ^{15}N-Ala data show a good fit for the single residue in the TMS, while an unresolved peak is seen for the three alanines in the APH, which agrees well with two out of the three predicted positions (Figure 3D). In the case of the ^{15}N-Leu-labeled sample, the signals of the APH are weak and poorly resolved in unflipped bicelles, but their visibility could be enhanced by flipping the bicelles. The three ^{15}N-Leu signals of the TMS are seen in the expected region and fit quite well in spectra of both unflipped and flipped bicelles. Since $TatA_{2-45}$ contains two leucines in the APH, which is preceded directly by Leu_{26}, we calculated the signals for all three residues as if they were part of a continuous helix. Leu_{26} (light blue in Figure 3E,F) and Leu_{37} are very close to each other, making it impossible to discriminate between them. The spectrum of the unflipped bicelles (Figure 3E) shows two signals, one of which fits well to Leu_{38}. The SAMMY spectrum of the flipped bicelles (Figure 3F), on the other hand, is much improved, as it now shows two signals that fit well to Leu_{26}/Leu_{37} and a third weak signal that fits to Leu_{38}.

Altogether, the spectral quality in the TMS region was excellent. The major source of deviation is the line width of the signals, from which we estimate the error in the azimuthal rotation angle to be within ±20° for the TMS. In the case of the APH, the error in ρ increases to ±50°, due to the relatively low signal-to-noise ratio and possible deviations from an ideal α-helical conformation.[50] Given that it was rather challenging to assign the APH signals in the SAMMY spectra of the selectively labeled samples, we critically assessed any potential error in the assignment by examining all possible parameter permutations in fitting the PISA wheel. Only the single alternative assignment noted above (based on Ile_{29}) showed a limited agreement between the experimental and fitted signals (see Figures S2 and S3), but the quality of this second-best fit is not as good as the preferred solution pursued below.

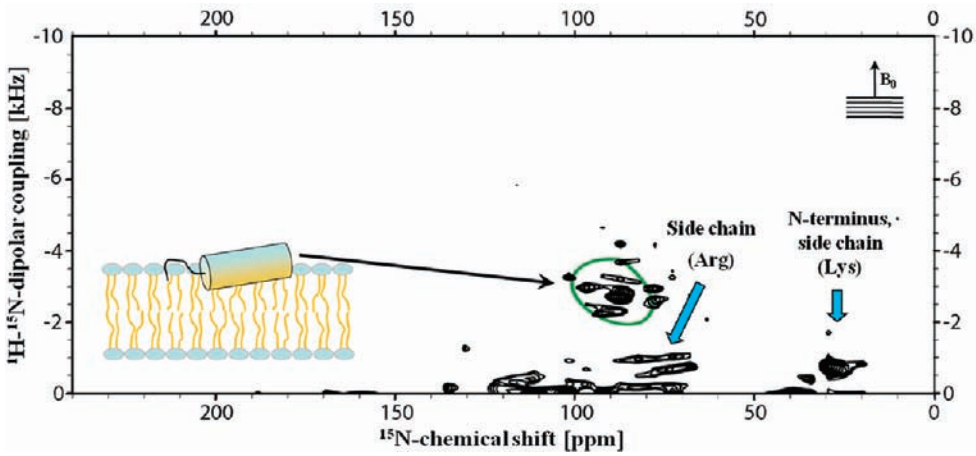

Figure 5. SAMMY spectrum of the uniformly ^{15}N-labeled APH ($TatA_{22-45}$) reconstituted in mechanically oriented bilayers on glass plates (DMPC/DMPG 30:70, P:L = 1:25, T = 315 K), overlaid with a simulated PISA wheel ($\tau = 81°$, $S_{mol} = 0.8$).

Nevertheless, as discussed in the Supporting Information, this alternative assignment does not change any of the basic conclusions on the TatA structure and its assembly mechanism proposed here.

The SAMMY spectrum of uniformly ^{15}N-labeled $TatA_{2-45}$ in unflipped bicelles is overlaid in Figure 4A with PISA wheels that have been simulated with the obtained order parameters, tilt and rotation angles. Any signals from amino acids for which it is not certain that they are part of the respective helices are marked with light color, and their labels are written in italics. For example, according to the D_2O exchange experiments by liquid-state NMR experiments (see Figure S1), the amino acids Ile_5, Gly_6, and Ile_7 do not seem to be part of the helix, but the SAMMY spectrum of the selective ^{15}N-Ile labels shows signals in the TMS region which very likely arise from Ile_5 and Ile_7. By heteronuclear NOE measurements in SDS micelles (data not shown), we found that Ser_{24}, Lys_{25}, and Leu_{26} are part of the hinge region, which is also supported by the structure reported by Hu et al.[50] The C-terminal amino acids Ser_{42}, Ala_{43}, Thr_{44}, and Lys_{45} are probably not so well folded in the APH of our truncated construct $TatA_{2-45}$ due to fraying.[73,74]

Based on these assignments, the helical wheel plots in Figure 4 depict the alignment of the TMS and the APH in the membrane as derived by solid-state NMR. Two notable features emerge from assessing these data. First, the membrane-embedded part of the hydrophobic TMS appears to be unusually short, consisting of only 13−15 residues according to liquid-state NMR (see Figure S1 and Hu et al.[50]), but the helix is extended toward the N-terminus. Second, the membrane alignment of the APH is quite unexpected. Compared to the usual behavior of a typical amphiphilic helix,[75,76] the APH has a comparatively steep tilt angle (instead of lying flat on the bilayer surface), and the observed azimuthal rotation places its polar face essentially sideways (instead of straight up or down).

2D NMR of Uniformly ^{15}N-Labeled $TatA_{22-45}$ on Glass Plates. The unexpected alignment of the APH raised the question whether this segment represents an independent structural entity within the TatA protein. If the APH was loosely connected to the TMS by a flexible hinge, its alignment would have to be intrinsically encoded in its local sequence. Alternatively, if the oblique structure of the APH is a functional feature of the TatA protein, then the observed alignment should be affected by the presence or absence of the hydrophobic TMS. Using our previous reductionist approach of studying separate segments of the TatA protein,[48] we now examined the membrane orientation of the isolated APH peptide, which was recombinantly produced as a ^{15}N-labeled fragment $TatA_{22-45}$. For this sample we employed mechanically oriented bilayers on glass plates as a membrane environment. Bicelles were avoided, because the APH does not possess a hydrophobic membrane anchor and might therefore preferentially bind to the bicelle rim like a detergent.

The SAMMY spectrum acquired with horizontally aligned glass plates in Figure 5 reflects the same sample geometry as the flipped bicelles. By analogy, the signals at 30 ppm in the ^{15}N-labeled APH ($TatA_{22-45}$) are assigned to the flexible N-terminus and the lysine side, and the signals at 70−90 ppm with very small dipolar couplings probably arise from the arginine side chains (as discussed above). The remaining group of signals around 75−100 ppm and with 2−4 kHz dipolar couplings must arise from the backbone amides of the APH. These signals form a PISA wheel that is not very well resolved, but computation clearly indicates a tilt angle of $\tau = 81° \pm 5°$. The simulated PISA wheel fits the overall signal distribution, and the order parameter is estimated as $S_{mol} \approx 0.8$, in good agreement with a monomeric peptide in a mechanically oriented sample. As expected for a "passive" amphiphilic, the isolated $TatA_{22-45}$ fragment is thus found to lie almost flat on the membrane surface. This orientation is clearly different from the alignment of the APH in the longer construct $TatA_{2-45}$ containing the TMS. These findings suggest that the APH is not just floating freely on the membrane surface as a flexible attachment to the TMS but probably plays an active role in the $TatA_d$ assembly and possibly in the mechanism of translocation. In the accompanying paper,[50] Hu et al. have shown by liquid-state NMR that $TatA_d$ possesses a well-structured hinge between TMS and APH, as residues Phe_{14}, Leu_{18}, Pro_{23}, and Leu_{26} assume a distinct local conformation and make extensive contacts with one another. It was also pointed out that this hinge region possesses the highest degree of conservation

(73) Welch, J. T.; Kearney, W. R.; Franklin, S. J. *Proc. Natl. Acad. Sci. U.S.A.* **2003**, *100*, 3725–3730.
(74) Fesinmeyer, R. M.; Peterson, E. S.; Dyer, R. B.; Andersen, N. H. *Protein Sci.* **2005**, *14*, 2324–2332.
(75) Bechinger, B.; Zasloff, M.; Opella, S. J. *Protein Sci.* **1993**, *2*, 2077–2084.
(76) Glaser, R. W.; Sachse, C.; Dürr, U. H. N.; Wadhwani, P.; Ulrich, A. S. *J. Magn. Reson.* **2004**, *168*, 153–163.

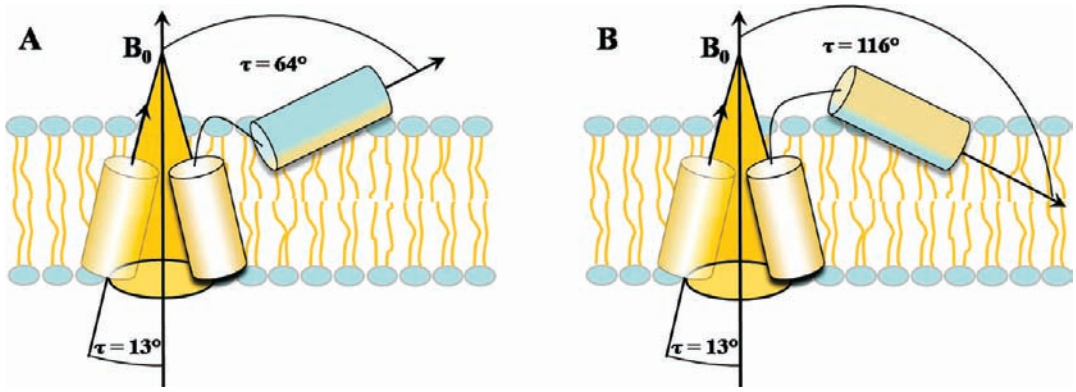

Figure 6. Two families of TatA$_{2-45}$ structures according to the helix orientations (τ_{TMS} and τ_{APH}) in the membrane as determined by solid-state NMR. The acyl chains, the TMS, and the predominantly hydrophobic face of the APH are colored yellow, while polar regions (lipid headgroups, hydrophilic face of the APH) are colored light blue.

among the TatA and TatB families, which implies an important biological function.

Discussion

TatA$_d$ is the pore-forming component in the minimal Tat-dependent translocation pathway of the Gram-positive bacterium *B. subtilis*, which consists of only the two proteins TatA$_d$ and TatC$_d$.[31] So far, little is known about the mechanism of this ATP-independent protein translocation pathway, and high-resolution structural data of these proteins are not available. Using a reductionist approach, we had previously examined various fragments of TatA$_d$ in the membrane-bound state by CD and OCD spectroscopy and were able to verify the predicted N-terminal transmembrane α-helix, the amphiphilic α-helix, and the unstructured C-terminus.[48] By solid-state NMR spectroscopy it was then possible to characterize the membrane alignment of the TMS as part of the relevant folded construct TatA$_{2-45}$, using oriented bicelles as a membrane environment.[49] Here, we have proceeded to determine the three-dimensional alignment of the APH in unflipped as well as flipped bicelles. By analyzing a range of different amino acid type-selective labels, it was also possible to refine the structure of the TMS and to assign the signal pattern of the APH. Two-dimensional separated local field NMR experiments were used to resolve the ^{15}N chemical shift/^{1}H−^{15}N dipolar coupling correlations. In these SAMMY spectra, the TMS of TatA$_{2-45}$ gives a well-resolved PISA wheel, whose simulation as an ideal α-helix reveals a tilt angle of $\tau = 13° \pm 4°$ and an order parameter of $S_{mol} \approx 0.8$. The rotation angle of the TMS is determined as $\rho_{Val15} = 235° \pm 20°$, with an error due also to the intrinsic signal width. The small differences in comparison to our previously estimated tilt and rotation angles of the TMS ($\tau \approx 17°$, $\rho_{Val15} \approx 215°$)[49] are within this limit and confirm the reproducibility among separate sample preparations and recordings. The refined rotation angle fits neatly to the entire range of selectively labeled samples measured here, which cover all the residues in the TMS (except for glycine). This amino acid type-selective labeling approach thus led to an assignment of the complete TMS and provides the necessary constraints for future structure calculations with atomic resolution. Apart from that, the selectively labeled samples showed that the membrane-embedded TMS is probably longer than the hydrophobic stretch seen by D_2O exchange experiments in detergent micelles using liquid-state NMR (see Supporting Information and Hu et al.[50]). The SAMMY spectra of a ^{15}N-isoleucine-labeled sample suggested that both Ile$_5$ and Ile$_7$ could be part of the TMS, with a slight perturbation at Ile$_7$ presumably due to the helix-breaker Pro$_8$.

The structure analysis of the APH was less straightforward than for the TMS, because the ^{1}H−^{15}N dipolar coupling is very small and changes its sign in this region of the SAMMY spectrum and signals are less well resolved. In addition to these difficulties, the APH gave significantly lower signal intensity compared to the TMS, presumably due to increased dynamics. To prevent further interference of signals from the unstructured C-terminus, we used the truncated construct TatA$_{2-45}$, which also showed much better orientation in bicelles than the full-length 70 amino acid protein. The NMR spectra of TatA$_{2-45}$ in magnetically oriented bicelles could be significantly improved by flipping them so that the bilayer normal was parallel to the field. The one-dimensional ^{15}N NMR spectra of TatA$_{2-45}$ in these flipped bicelles showed increased signal intensity in the APH region and better resolution due to the doubling of the spectral width. Comparison of the flipped and unflipped samples further allowed us to assign the highly mobile side chains, as their signals remain close to the isotropic position upon flipping. This way, the amide signals from the backbone of the APH could be identified, which do not actually look like those of a ring but can be attributed to a folded PISA wheel that changes its sign. By fitting an ideal α-helix to the measured signal distribution, the tilt angle of the APH was determined to be $\tau = 64° \pm 10°$, $\rho_{Ile29} = 25° \pm 50°$, with a molecular order parameter of $S_{mol} \approx 0.5$. Compared to the TMS ($S_{mol} \approx 0.8$), the attached APH thus possesses a higher mobility than the transmembrane anchor.

From the two fully characterized TMS and APH segments, it should be possible now to assess the overall architecture of the protein TatA$_d$ in the membrane-bound state. Due to the intrinsic inversion symmetry of the NMR tensors, however, there still exists a fundamental ambiguity. Namely, when describing the membrane alignment of a chiral protein segment from several independent NMR constraints, the angular pair $[\tau, \rho]$ is equivalent to $[180° - \tau, 180° + \rho]$.[77] Once the upper and lower bilayer faces are defined by the directionality of the N-terminal TMS, the two mathematical solutions for the APH may be regarded as placing this helix either face-up or face-down into the monolayer leaflet. For a normal amphiphilic helix, it is usually intuitively clear which of the two descriptions is compatible with hydrophobicity considerations. However, as the present APH is oriented in an unusual way, we should consider both mathematically allowed solutions, which correspond to physically different membrane interactions. Namely, we can link

(77) Strandberg, E.; Esteban-Martín, S.; Salgado, J.; Ulrich, A. S. *Biophys. J.* **2009**, *96*, 3223–3232.

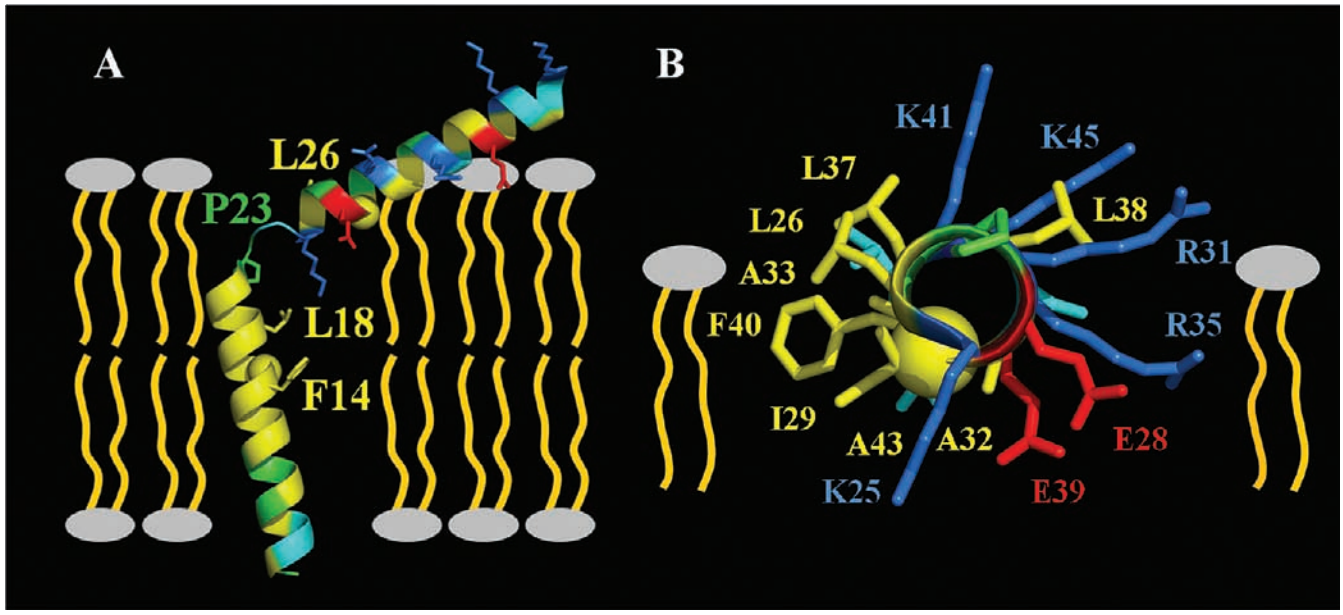

Figure 7. Three-dimensional model of $TatA_{2-45}$ embedded in the lipid bilayer. (A) The N-terminal TMS and the amphiphilic APH are depicted as straight helices, whose membrane alignment was determined by solid-state NMR and whose intramolecular angle is depicted according to liquid-state NMR. The Cα-atoms of Val_{15} and Ile_{29} are marked with balls to depict the azimuthal rotation angle of the two helices. All charged side chains are shown explicitly, as well as those for which intramolecular NOEs have been reported. (B) Illustration of the azimuthal alignment of the APH, where salt-bridges might be formed between Lys_{25} and Glu_{28}, and possibly Glu_{39} and Arg_{35}.

the TMS [$\tau_{TMS} = 13°$, $\rho_{Val15} = 235°$] with an APH of either [$\tau_{APH} = 64°$, $\rho_{Ile29} = 25°$] or [$\tau_{APH} = 116°$, $\rho_{Ile29} = 205°$]. Furthermore, each helix is defined with respect to only a single reference axis in the *z*-direction, i.e., the membrane normal, but the rotation in the $x-y$ plane remains undetermined. Therefore, both allowed combinations of APH and TMS are undefined in terms of the intramolecular angle Δ_{TMS} between the two helical segments, as illustrated in Figure 6. As a result, the solid-state NMR data alone can resolve the membrane-bound structure of TatA only up to the point where there are two discrete families of solutions.

To select the unique solution from the continuum of structures lying on the cones in Figure 6, additional conformational criteria need to be obtained by an independent method. First, it would help to know the intramolecular angle Δ_{TMS} between the two helical segments, as this would leave four solutions at most. According to our present constraints, this angle is allowed to range from [$180° - \tau_{TMS} - \tau_{APH}$] to [$180° + \tau_{TMS} - \tau_{APH}$], corresponding to values of $\Delta_{TMS} = 103° \pm 14°$ to $\Delta_{TMS} = 129° \pm 11°$ for the arrangement in panel A of Figure 6 (where $\tau_{APH} = 64°$) and $\Delta_{TMS} = 51° \pm 14°$ to $\Delta_{TMS} = 77° \pm 11°$ in panel B (where $\tau_{APH} = 116°$). In the liquid-state NMR analysis of $TatA_d$ by Hu et al.,[50] an L-shape structure was observed in detergent micelles, in which the two helices enclose an angle of about $\Delta_{TMS} \approx 90°$. If this constraint is applied to the two families of solid-state NMR structures, visual inspection of Figure 6 shows that only two solutions remain. In panel A of Figure 6, only the smallest possible angle ($\Delta_{TMS} \approx 103° \pm 11°$) is compatible with both the solid-state and liquid-state NMR data, and in panel B, only the largest possible value ($\Delta_{TMS} \approx 77° \pm 11°$) can be considered as a feasible solution.

To discriminate these two possibilities, we can further use the fact that intramolecular NOEs have been reported for the full-length $TatA_d$ in DPC micelles, namely between Phe_{14}, Leu_{18}, and Pro_{23} on the TMS and Leu_{26} on the APH.[50] Likewise, our own liquid-state NMR analysis in SDS micelles (data not shown) has revealed a distinct NOE between Leu_{18} and Pro_{23} in the same truncated $TatA_{2-45}$ construct used here for solid-state NMR. These conserved contacts clearly support the arrangement in Figure 6A with $\Delta_{TMS} \approx 103°$, where $\rho_{Val15} = 235° \pm 20°$ and $\rho_{Ile29} = 25° \pm 50°$. This unique solution is illustrated in Figure 7, and it also agrees much better with the amphiphilic faces of the APH than the other formal possibility illustrated in Figure 6B. The molecular picture obtained here is close to the arrangement of the helices determined from RDCs in detergent micelles.[50] Altogether, by combining the constraints from liquid-state and solid-state NMR, the three-dimensional structure of TatA has thus been fully resolved, including its detailed molecular conformation and its global alignment in the lipid membrane.

Conclusions

A notable aspect of the TatA structure obtained here is the finding that the APH is aligned with a comparatively steep tilt angle in the membrane (rather than flat) and that its azimuthal rotation places the polar residues more or less sideways (rather than upward), as seen in Figure 7. It seems as if the unusually short hydrophobic TMS of only 14 amino acids length pulls the N-terminus of the APH quite deeply into the membrane and that the well-structured hinge between the two helices induces the peculiar azimuthal angle. The proposed structure allows the hydrophobic patch at the N-terminal end of the APH (Leu_{26}, Ile_{29}, Ala_{33}, and Leu_{37}) to be favorably immersed in the bilayer core. At the same time, however, the charged residues of Lys_{25} and Glu_{28} would be exposed to such a hydrophobic environment. Since there exist no lipids that could compensate for the negative charge on Glu_{28}, we speculate that it might be stabilized by forming an intramolecular salt-bridge with Lys_{25}, which is situated adjacently in the loop (or, as in the simplified drawing of Figure 7, at the end of the straight helix). Further toward the middle of the APH, the long cationic side chains of Arg_{31} and Arg_{35} should readily be able to "snorkel" upward and interact with anionic phospholipid headgroups.[78,79] At the C-terminal end, Glu_{39}, Lys_{41}, and Lys_{45} are favorably close to the aqueous layer, though again with Glu_{39} pointing sideways, where it might

form a salt-bridge with Arg_{35}, depending on the depth of immersion (which cannot be addressed here by either solid-state or liquid-state NMR). In this terminal region of the APH, we note that the solvent-exposed Leu_{38} is an intrinsic part of the polar face; hence, it might play a specific role in the function of TatA.

Being the most prominent part of the twin-arginine translocation system, TatA is believed to self-assemble into a large channel, across which fully folded proteins can be translocated. The monomeric TatA structure proposed here represents an essential step toward constructing such an oligomeric complex. Given the observed alignment of the APH in the membrane, it does not seem to be just a flexible attachment to the TMS, but instead it assumes an oblique, skewed tilt angle in the membrane. The resulting distribution of polar residues in the lipid bilayer can be considered as stable by postulating the formation of one or two intramolecular salt-bridges, which are sterically feasible (see Figure 7). It is tempting to speculate that the charged side chains on the APH might play a role in the self-assembly of TatA by forming *inter*molecular salt-bridges between adjacent monomers. We note that the APH of TatA is predominantly cationic, while the C-terminus is predominantly anionic,[80] hence, an oligomerization in the membrane might be envisaged via electrostatic interactions. To verify this hypothesis, a mutagenesis study, which would have to include functional translocation assays, would be an interesting topic for future structural and mechanistic investigations on oligomeric TatA. In the present NMR analysis, the unstructured C-terminus had been removed to significantly improve the spectral quality, and our construct $TatA_{2-45}$ indeed behaved like a monomer, as evident, e.g., from its rotational diffusion in the membrane. In the accompanying liquid-state NMR analysis of the full-length protein,[50] Hu et al. did not detect any self-assembly either, as it was solubilized in detergent micelles. It would thus be exciting to explore whether TatA can self-assemble in the membrane-bound state, using a high protein concentration under optimized conditions to observe an oligomeric pore structure.

Material and Methods

Expression and Purification. The cloning and expression of different $TatA_d$ constructs have been previously described by Lange et al.[48] The expression of uniformly and selectively labeled protein for NMR experiments has been described by Müller et al.[49] The present work was carried out with the well-structured construct $TatA_{2-45}$ and with the isolated APH ($TatA_{22-45}$) (full protein sequence: MFSNIGIPGL$_{10}$ ILIFVIALII$_{20}$ FGPSKLPEIG$_{30}$ RAAGRTLLEF$_{40}$ KSATKSLVSG$_{50}$ DEKEEKSAEL$_{60}$ TAVKQD-KNAG$_{70}$). The genes of all fragments were cloned in a pET-28a(+) vector (Novagen, Merck, Germany), which codes for an N-terminal His_6-tag to facilitate purification. The TatA constructs were expressed in *E. coli* BL21 cells (Novagen, Merck, Germany) in M9 minimal medium[81] at 37 °C and 200 rpm shaking frequency, with $^{15}NH_4Cl$ as the sole nitrogen source. Induction was done at an $OD_{600} = 0.6-0.9$ with IPTG, and cells were allowed to express for 20 h, or for 2−4 h for selectively labeled samples. For amino acid type-selective labeling, we used $^{14}NH_4Cl$ and a mixture of all unlabeled amino acids (200−500 mg) plus the ^{15}N-labeled one (100 mg), which was added 30 min before induction. Cells were disrupted by sonification, and the protein was solubilized with the help of the detergent *N*-lauroyl-sarcosinate (NLS) (Fluka, Sigma-Aldrich, Germany) from the cell debris and membrane. The solubilized protein was purified using Ni-NTA affinity chromatography in the presence of NLS. The protein was dialyzed to remove the detergent prior to CNBr cleavage, which was carried out in 50% TFA to yield the fragments $TatA_{2-45}$ or $TatA_{22-45}$. The CNBr cleavage mixture was lyophilized, and the powder was solubilized with 2% NLS in the case of $TatA_{2-45}$, or with 0.5% NLS in the case of $TatA_{22-45}$. The low NLS concentration in the case of $TatA_{22-45}$ prevents the solubilization of the TMS part, which was produced from the precursor $TatA_{2-45F21M}$ during CNBr cleavage. A subtractive Ni-NTA affinity chromatography step was carried out to remove the His_6-Tag and uncleaved protein. An exhaustive dialysis then followed to remove the NLS, whereupon the protein $TatA_{2-45}$ precipitates and $TatA_{22-45}$ stays mainly in solution. Lyophilization yielded the respective protein as a white powder, with average yield of about 25 mg/L for $TatA_{2-45}$ and 15 mg/L for $TatA_{22-45}$. The purity of the protein was checked by MALDI-TOF and SDS-PAGE.

Sample Preparation. The reconstitution of $TatA_{2-45}$ into bicelles has been described by Müller et al.,[49] and the general bicelle preparation was described by De Angelis et al.[52] We used DMPC and DMPG as long-chain lipids and the ether-linked 6-O-PC as a short-chain lipid to improve the stability of the bicelles. The long-chain lipids were weighed as a dry powder (Avanti Polar Lipids, USA) to a molar ratio of 80:20 (DMPC:DMPG). The lipid 6-O-PC (Avanti Polar Lipids, USA) was added to this dry powder as a stock solution in water to yield a long-chain to short-chain lipid ratio of $q = 3.2$ (56 mg lipid in total). Next, 200 μL of H_2O was added, and the mixture was vortexed extensively at 0 and 43 °C alternatingly until it became clear. The pH was adjusted to pH = 6.8 at 0 °C, and 170 μL of the bicelles was added to $TatA_{2-45}$ to yield a molecular ratio of 1:100. The mixture was vortexed again at 0 and 43 °C until the protein dissolved, and the pH was checked once more. Afterward, the bicelles were transferred to a flat-bottomed glass tube with 5 mm outer diameter (New Era Enterprises, USA) and sealed tightly with a rubber plug.

To prepare mechanically oriented samples on glass plates, we weighed out DMPC and DMPG as a dry powder in a molar ratio of 30:70 (19.8 mg total lipid). We used a high proportion of negatively charged lipids, as they gave better spectra for the construct $TatA_{22-45}$. The lipids were dissolved in chloroform/methanol and subsequently dried under a stream of nitrogen gas to yield a dry lipid film. Residual organic solvent was removed under high vacuum overnight. The lipid film was hydrated with H_2O and sonicated to give small unilamellar vesicles. The protein $TatA_{22-45}$ was added to this solution to yield a molecular ratio of 1:25, and the solution was incubated for 30 min at 37 °C. We used such a high molecular ratio because of the small molecular weight of this construct and because the smaller amount of lipids compared to bicelles leads to a lower sensitivity. The solution was distributed equally over 22 glass plates (7.5 × 12 mm), which were stacked after drying, and subsequently rehydrated using saturated K_2SO_4 solution at 48 °C and 97% relative humidity overnight. Afterward the stack was transferred to a glass container (7.7 × 2.2 × 30 mm) (New Era Enterprises, USA), and to prevent drying, a water reservoir (paper soaked with 75 μL of H_2O) was added and the opening sealed with parafilm.

Solid-State NMR. NMR spectra were recorded on a Bruker 500 MHz Avance III spectrometer (Bruker Biospin, Germany) equipped with a Bruker HXY probe (5 mm inner diameter round solenoid coil) or on a Bruker 500 MHz Avance spectrometer with a wide-bore 500/89 AS Magnex magnet (Yarnton, UK) equipped with a home-built $^1H-^{15}N$ probe (5 mm inner diameter round solenoid coil). All spectra were referenced in the ^{15}N dimension to solid

(78) Strandberg, E.; Killian, J. A. *Febs Lett* **2003**, *544*, 69–73.
(79) Segrest, J. P.; Loof, H. D.; Dohlman, J. G.; Brouillette, C. G.; Anantharamaiah, G. M. *Proteins* **1990**, *8*, 103–117.
(80) Warren, G.; Oates, J.; Robinson, C.; Dixon, A. M. *J. Mol. Biol.* **2009**, *388*, 122–132.
(81) Cai, M.; Huang, Y.; Sakaguchi, K.; Clore, G. M.; Gronenborn, A. M.; Craigie, R. *J. Biomol. NMR* **1998**, *11*, 97–102.

NH_4SO_4 (26.8 ppm, which corresponds to 0 ppm for liquid ammonia)[82] and in the ^1H dimension to H_2O (4.7 ppm at 42 °C).

The quality of protein reconstitution and the alignment of the membrane-mimicking environment were checked by a 1D ^{31}P NMR prior to every ^{15}N NMR measurement. The 1D$-^{15}N$ NMR spectra were recorded with cross-polarization and the CP-MOIST pulse sequence.[83] During acquisition, heteronuclear ^1H-decoupling was achieved using the SPINAL-16 composite pulse sequence with a field strength of 30 kHz.[84,85] A 1 ms cross-polarization contact time and a recycle delay of 6−8 s were used to avoid sample heating, for both one- and two-dimensional experiments.

For ^{15}N chemical shift/$^1H-^{15}N$ dipolar coupling correlation spectra, we used the SAMMY experiment[58] with the improved pulse sequence SAMPI4.[59] The proton carrier frequency was set to 9 ppm and the ^{15}N carrier frequency to 88 ppm (in unflipped bicelles), 150 ppm (in flipped bicelles), or 110 ppm ($TatA_{22-45}$ reconstituted in mechanically aligned bilayers on glass plates). We used a ^1H $\mathbf{B}_1$ field strength of 51 kHz, and during the 10 ms acquisition time a 30 kHz decoupling was applied. The received data sets were zero-filled, and the $^1H-^{15}N$ dipolar coupling dimension was scaled as described in ref 59. For processing and display of the data, we used the programs NMRPipe,[86] SPARKY,[87] and TOPSPIN (Bruker-Biospin, Germany).

Simulations. To determine the tilt angle τ, the order parameter S_{mol}, and the rotation angle ρ, we calculated simulated PISEMA spectra and compared them with the experimental signal patterns. For the simulation of PISA wheels, we used a home-written program (S. Grage, KIT). All simulations were performed for an ideal α-helix with uniform dihedral angles ($\Phi = -60.7°$; $\Psi = -44.7°$), uniform chemical shift tensor principal components ($\sigma_{11_N} = 64$ ppm; $\sigma_{22_N} = 77$ ppm; $\sigma_{33_N} = 222$ ppm), a N−H bond length of 1.07 Å, and a uniform angle of $\delta = 18.5°$ between the principal component σ_{33_N} and the NH vector.[49,88] It was justified to use average principal components of the chemical shift tensor and an average angle δ, because their influence on the overall helix orientation is low.[60,89] As molecular visualization software, PyMOL was used.[90]

Acknowledgment. This work was supported by the Karlsruhe House of Young Scientists with a "KHYS Auslandsstipendium" and by the CFN projects E3.4 and E1.2. We are most grateful to Stanley Opella for his advice and access to the Biomedical Technology Resource for NMR Molecular Imaging of Proteins at the University of California, San Diego (supported by NIH grant P41EB002031), to Fabian Filipp for his personal guidance and engagement, and to Francesca Marassi for NMR time at the Sanford Burnham Institute, La Jolla. We thank Claudia Muhle-Goll for her advice on liquid-state NMR and access to unpublished data, Sergii Afonin for MALDI sample characterization, and Sonja Müller for some of the labeled material.

Supporting Information Available: Figure S1, D_2O exchange experiments in SDS micelles to determine the length of the TMS by liquid-state NMR; Figure S2, SAMMY spectra of selectively ^{15}N-labeled $TatA_{2-45}$ bicelles to illustrate the alternative assignment of the APH; Figure S3, alternative assignment of the APH illustrated in the spectrum of the uniformly labeled sample, and illustration of the resulting structure and alignment of TatA in the membrane; complete ref 72. This material is available free of charge via the Internet at http://pubs.acs.org.

JA106963S

(82) Wishart, D. S.; Bigam, C. G.; Yao, J.; Abildgaard, F.; Dyson, H. J.; Oldfield, E.; Markley, J. L.; Sykes, B. D. *J. Biomol. NMR* **1995**, *6*, 135–140.
(83) Levitt, M. H.; Suter, D.; Ernst, R. R. *J. Chem. Phys.* **1986**, *84*, 4243–4255.
(84) Sinha, N.; Grant, C. V.; Wu, C. H.; De Angelis, A. A.; Howell, S. C.; Opella, S. J. *J. Magn. Reson.* **2005**, *177*, 197–202.
(85) Fung, B. M.; Khitrin, A. K.; Ermolaev, K. *J. Magn. Reson.* **2000**, *142*, 97–101.
(86) Delaglio, F.; Grzesiek, S.; Vuister, G. W.; Zhu, G.; Pfeifer, J.; Bax, A. *J. Biomol. NMR* **1995**, *6*, 277–293.
(87) Goddard, T. D.; Kneller, D. G. *SPARKY*; University of California, San Francisco.
(88) De Angelis, A. A.; Howell, S. C.; Nevzorov, A. A.; Opella, S. J. *J. Am. Chem. Soc.* **2006**, *128*, 12256–12267.
(89) Brender, J. R.; Taylor, D. M.; Ramamoorthy, A. *J. Am. Chem. Soc.* **2001**, *123*, 914–922.
(90) *PyMOL*, Version 1.2r3pre ed; Schrödinger LLC, 2010.